International Journal of Refractory Metals and Hard Materials 111 (2023) 106054

Contents lists available at ScienceDirect

International Journal of Refractory Metals and Hard Materials

journal homepage: www.elsevier.com/locate/IJRMHM

In situ powder X-ray diffraction during hydrogen reduction of MoO_3 to MoO_2

M. Burgstaller [a], H. Lund [b], M. O'Sullivan [c], H. Huppertz [a,*]

[a] Institute of General, Inorganic, and Theoretical Chemistry, University of Innsbruck, Innrain 80-82, 6020 Innsbruck, Austria
[b] Leibniz-Institute for Catalysis e.V, Albert-Einstein-Straße 29a, 18059 Rostock, Germany
[c] Plansee SE, Metallwerk-Plansee-Straße 71, 6600 Reutte, Austria

ARTICLE INFO

Keywords:
Molybdenum oxide
In situ X-ray powder diffraction
Hydrogen reduction
Potassium

ABSTRACT

The hydrogen reduction of molybdenum trioxide to molybdenum dioxide is not yet fully understood as evident by continuous scientific interest. Especially the effect of the potassium content on the reduction process has not yet been considered. We prepared several samples of molybdenum trioxide containing varying amounts of potassium by addition of potassium molybdate (K_2MoO_4). *In situ* powder X-ray diffraction experiments were then conducted to study the hydrogen reduction of these samples. We especially focused on the influence of the alkali content and on gaining insight into the importance of the intermediary product γ-Mo_4O_{11}. During the reduction process, MoO_2 is formed from the reduction of MoO_3, which then reacts with the starting material to form γ-Mo_4O_{11}. With increasing potassium content, the reduction rate is decreased and the fractional content of γ-Mo_4O_{11} built up during the reduction process is increased. As evident from bulk sample reduction, this results in a significant increase in the grain size visualized *via* scanning electron microscopy. Our investigations once again underline the importance of γ-Mo_4O_{11} on the morphology of the resulting MoO_2 powder.

1. Introduction

Molybdenum and its oxides are of crucial importance in the refractory metal industry, *e.g.* in the alloying of steel [1] and heterogeneous catalysis for selective oxidation of olefins [2,3]. Additionally, molybdenum is used in many applications like sputtering targets for flat panel displays [4], semiconductor base plates [5] or anodes for X-ray tubes, which are of considerable importance in the medical field today [6]. On industrial scales, elemental molybdenum is prepared by the reduction of molybdenum trioxide through hydrogen [7]. According to Eq. (1), this is a two-step process propagating at temperatures of 500–700 °C and 950–1150 °C, respectively.

$$MoO_3 \rightarrow MoO_2 \rightarrow Mo \quad (1)$$

The morphology of the molybdenum product is thereby at least partially dependent on the morphology of the intermediary product MoO_2 [8]. The molybdenum dioxide is obtained after the first reduction step *via* a chemical vapor transport (CVT) [9]. The parallel/intermediary product γ-Mo_4O_{11} (henceforth called Mo_4O_{11} for brevity) is developed at reduction temperatures >440 °C [8] and has a profound impact on the habitus of the developed molybdenum dioxide [10]. Important influencing factors, such as temperature and dew point of the reduction gas were identified early on [9,11–13].

The *in situ* neutron powder diffraction of a 10 g sample was reported by Lalik et al. [14]. The experiments clearly showed the appearance of Mo_4O_{11} during the reduction process. While the initial reduction yielded the molybdenum dioxide, it quickly resulted in a plateau of the MoO_2 phase, while more and more Mo_4O_{11} was developed, reaching a maximum at a fractional content of ~85%. These exceptional findings gave a first glimpse on the importance of the Mo_4O_{11} phase. Further *in situ* powder X-ray diffraction (XRD) experiments by Leisegang et al. [15] showed the existence of two separate molybdenum trioxide phases, with fractional contents dependent on the experienced temperature and a reduction kinetic governed by the crystallite size of the MoO_3 sample. In comparison, large crystallites exhibited less stability and preferred intercalation of hydrogen to form molybdenum bronzes, as well as preferred reaction to Mo_4O_{11}.

The intercalation of hydrogen into the molybdenum trioxide framework was intensely studied by Borgschulte et al. [16], while reducing molybdenum trioxide at room temperature. The *in situ* XPS analyses clearly showed, that depending on the experimental conditions, a multitude of reduction pathways can occur. At very low temperatures,

* Corresponding author.
E-mail address: hubert.huppertz@uibk.ac.at (H. Huppertz).

https://doi.org/10.1016/j.ijrmhm.2022.106054
Received 27 September 2022; Received in revised form 16 November 2022; Accepted 24 November 2022
Available online 26 November 2022

the formation of molybdenum bronzes (H_xMoO_3) prior to reduction occurs, which was also reported by Ressler et al. [17]. However, the formation of bronzes becomes less significant with higher temperatures. At increased temperatures, the reaction follows a direct path according to reaction Eq. (2), as this is the energetically favored reaction path. With further increased temperature, the molybdenum oxide Mo_4O_{11} is observed [17]. Incidentally, during the reduction with pure hydrogen and a reduction temperature of 550 °C, the *in situ* developed Mo_4O_{11} phase content rises to a maximum of ~15%. The origin of the developed Mo_4O_{11} is currently still debated as some researchers [18,19] favor the reaction of molybdenum dioxide and starting material according to Eq. (3), while several others [20,21] support the consecutive reaction mechanism described by Eqs. (4) and (5), where Mo_4O_{11} is developed as an intermediary reaction product. Additionally complicating the matter, a competitive nucleation [14] approach with at least two parallel routes of molybdenum dioxide formation is discussed as well.

$$MoO_3 + H_2 \rightarrow MoO_2 + H_2O \tag{2}$$

$$3MoO_3 + MoO_2 \rightarrow Mo_4O_{11} \tag{3}$$

$$4MoO_3 + H_2 \rightarrow Mo_4O_{11} + H_2O \tag{4}$$

$$Mo_4O_{11} + 3H_2 \rightarrow 4MoO_2 + 3H_2O \tag{5}$$

The specific rate limiting step of the reaction mechanism is dependent on the reaction temperature as well [22]. Experiments conducted by Wang et al. [23] confirmed the importance of Mo_4O_{11} by the synthesis of uniform and large MoO_2 grains through a temperature controlled heating program utilizing a low-high-low temperature profile. The fractional content of Mo_4O_{11} produced during the reduction process was thereby maximized, yielding the desired morphological parameters to ultimately obtain molybdenum particles with a superior sintering performance. As we have reported in an earlier publication [24], we were able to consistently synthesize molybdenum dioxide samples with predefined morphologies ranging from small platelets to large cuboid like structures. This was possible through the increase of the potassium content by adding small amounts of potassium molybdate. Further investigations into the reaction mechanism by *in situ* powder X-ray diffraction reduction of molybdenum trioxide samples containing 34 and 120 µg K^+/g MoO_3, respectively, are discussed in the following.

2. Experimental

2.1. Sample preparation

Pure molybdenum trioxide (MoO_3) powder with a native potassium (K^+) content of 34 µg K^+/g MoO_3 supplied by Molymet S.A. (San Bernardo, Chile) was used for the experiments. A thorough characterization of the starting material was done in an earlier publication [24]. Samples with higher potassium contents were prepared by addition of a 100 µg K^+/ml H_2O containing standard solution (prepared from K_2MoO_4). Subsequent to addition of the standard solution, the emulsion was mixed and the residual water was evaporated in a kiln at 90 °C.

2.2. In situ powder X-ray diffraction

In situ XRD studies were performed on a Stoe Stadi P equipped with a Stoe ht2 *in situ* oven and a Mythen 1 K detector in Debye-Scherrer geometry using monochromatized Mo-$K\alpha_1$ radiation (50 kV, 40 mA, λ = 70.930 pm). The sample to investigate was ground, pressed to pellets at a pressure of 10 tons, crushed, and sieved to a fraction of 100–150 µm. A specimen was filled into a quartz glass capillary (approx. 2 mm outer diameter, 1 mm inner diameter, open on both sides) until a height of approx. 6 mm was achieved and fixed by quartz glass wool.

In the case of data collection under inert conditions the capillary was flushed with He (10 ml/min), heated to the desired temperature and diffraction data were collected after 5 min of equilibration time. In the case of *in situ* reduction monitoring, the capillary was flushed with He (10 ml/min) and the sample was heated to the desired temperature (10 °C/min). After equilibration, the gas feed was changed to H_2 (10 ml/min) and the reduction was monitored using static data collection over a 17° angular region for either 120 s (550 °C) or 30 s (700 °C). Gas dosage was done *via* a set of Bronkhorst mass flow controllers. Applied temperature correction function was received by observation of well-known phase transitions ($AgNO_3$, $KClO_4$, Ag_2SO_4, SiO_2, K_2SO_4, K_2CrO_4, WO_3, $BaCO_3$).

2.3. Phase composition calculation

To obtain the semi-quantitative phase composition, the intensity of the main reflections (*hkl*) of all four phases MoO_3 (*110*) [25], Mo_4O_{11} (*211*) [26], MoO_2 (*011*) [15], and Mo (*hkl* = *011*) [27]) were determined from the powder X-ray diffraction measurement of each data point. The constant background contribution was subtracted from the main reflection of each phase and the fractional phase content X_P was then calculated from the relative reflection intensities r*RI* according to Eq. (6), giving a good estimate of the fractional content.

$$X_P = \frac{rRI_P}{rRI_{MoO_3} + rRI_{Mo_4O_{11}} + rRI_{MoO_2} + rRI_{Mo}} \tag{6}$$

However, as only crystalline phases can be determined with the X-ray diffraction experiments, no assertion of the complete powder composition (*e.g.* non-crystalline phases) and the gaseous species can be confidently made.

3. Results

While heating the molybdenum trioxide sample to the set reduction temperature, X-ray diffraction experiments were conducted at selected temperatures. The resulting powder diffraction patterns are shown in Fig. 1. The distinct contribution of the experimental setup is noticeable in the range $7° < 2\theta < 13°$ (Mo-$K\alpha_1$; λ = 70.93 pm) by a broad background that is constant throughout the measurements. The most distinct reflections of MoO_3 are found in the region of $10.5° < 2\theta < 13°$. Most notably, an additional reflection develops with increasing temperature at 2θ = ~11.8°.

Furthermore, as a result of the anisotropic expansion of the lattice parameters, preferentially along the *b*-axis, the (*020*), (*040*), and (*060*) reflections (indicated in the 700 °C measurement) are shifted to lower angles, which is consistent with the literature [28]. At such high temperatures, the sample undergoes constant sublimation and recrystallization inside the capillary, further complicating the measurements and preventing reduction experiments at even higher temperatures. The additional reflection at 2θ = ~10.4° as well as the pronounced asymmetry of the *021* reflection (2θ = ~12.4°) is presumably caused by an additional MoO_3 phase as described by Leisegang et al. [15].

For all X-ray diffraction patterns, a Rietveld refinement was conducted and the change of the lattice parameters in dependence on the temperature is depicted in a graphical format in Fig. 2 (left). With increasing temperature, the lattice volume increases about 4% from 0.20259(3) nm^3 at 100 °C to 0.21097(3) nm^3 at 700 °C. The lattice parameters *a* and *c* undergo only minor variations when increasing the temperature from 100 to 700 °C. The *a*-axis length increases ~0.8% from 395.63(3) pm to 398.90(3) pm, while the *c*-axis length decreases ~0.2% from 368.92(2) pm to 368.25(3) pm. The enlargement of the cell volume is driven mainly by the increase in the *b*-axis length of ~3.5% from 1388.0(1) pm to 1436.2(1) pm.

The coefficient of thermal expansion α_V is derived from the linear expansion coefficient [29] in Eq. (7) and calculated for 700 °C yielding $\alpha_a = 1.4 \cdot 10^{-5}\,K^{-1}$, $\alpha_b = 5.8 \cdot 10^{-5}\,K^{-1}$, $\alpha_c = -0.3 \cdot 10^{-5}\,K^{-1}$, and $\alpha_V = 6.9 \cdot 10^{-5}\,K^{-3}$, which is in good agreement with the literature [28].

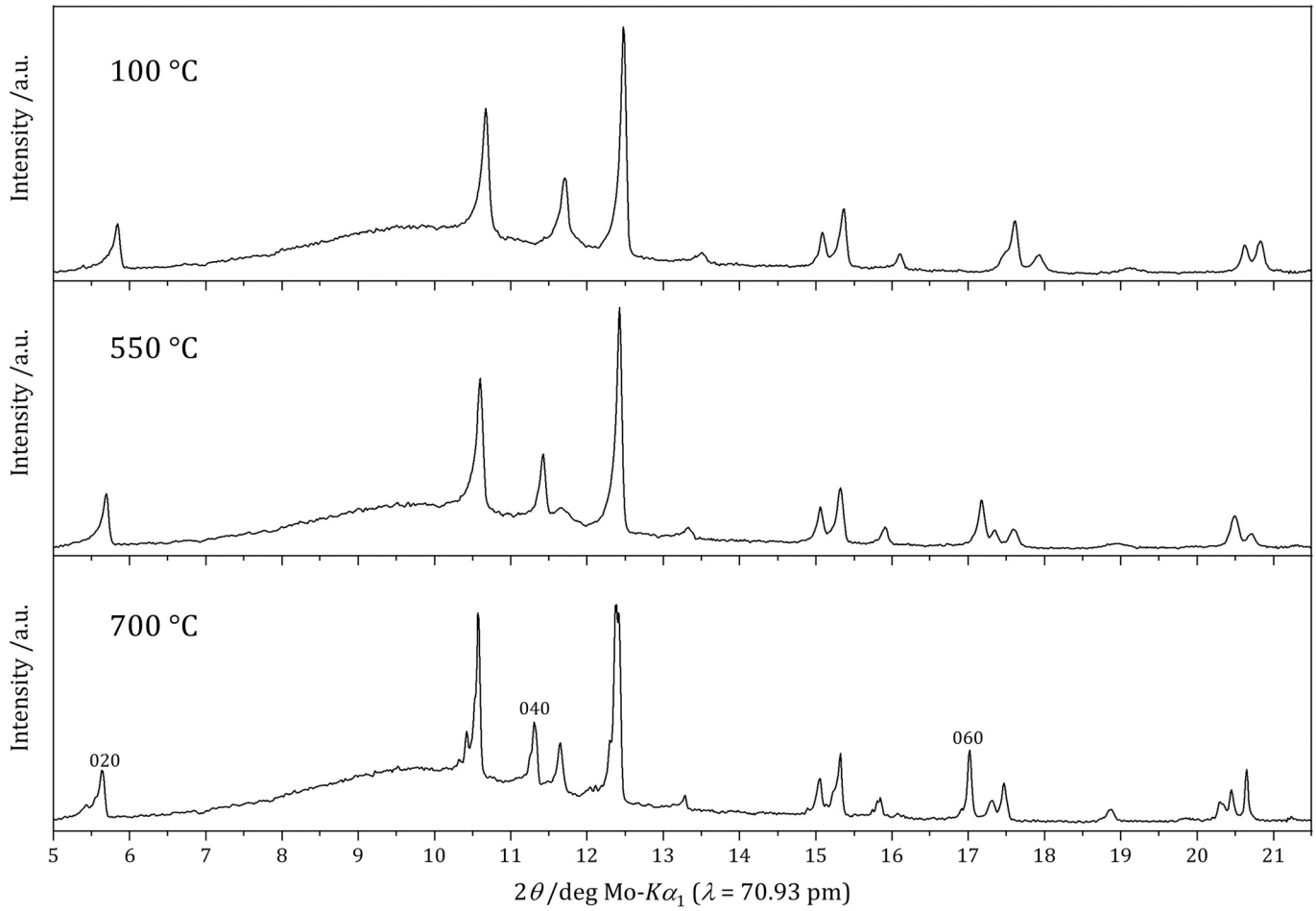

Fig. 1. Temperature dependant evolution of the X-ray diffraction pattern of α-MoO_3 at 100, 550, and 700 °C, respectively.

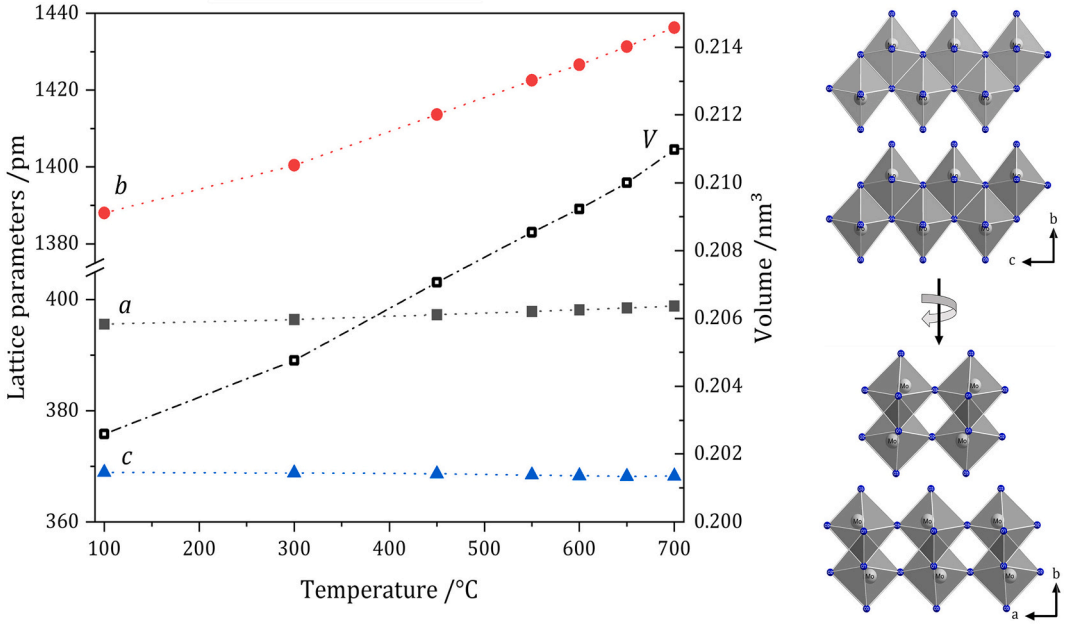

Fig. 2. Left: Lattice parameter evolution calculated from X-ray diffraction experiments and Rietveld refinement. Right: "Zigzag" structural motif of MoO_3 depicted along the a-axis (top) and along the c-axis (bottom).

$$\alpha_x = \frac{1}{x}\frac{dx}{dT} \tag{7}$$

An overview of the layer-like molybdenum trioxide structure consisting of "zigzag" planes stacking along the *a*-axis (top) and along the *c*-axis (bottom) is depicted in Fig. 2 (right). Two layers of molybdenum trioxide polyhedra are separated by the van-der-Waals gap [30], which increases from 266.62(1) pm at 100 °C to 275.87(1) pm at 700 °C.

The raw data of the hydrogen reduction of molybdenum trioxide samples containing 34 (left) and 120 (right) µg K^+/g MoO_3 at 550 °C is depicted in Fig. 3. During the hydrogen reduction of the sample containing 34 µg K^+/g MoO_3, the first indication of the reduction process is discernable with the second data point (t = 2 min) as molybdenum trioxide is reduced to molybdenum dioxide. After the initial reduction, the phase content of the molybdenum dioxide rises continuously. However, after the occurrence of the MoO_2 phase, Mo_4O_{11} reflections appear at t = 8 min. Both phases are then developed parallel to each other until the starting material is fully reacted. Afterwards, the Mo_4O_{11} is reduced to molybdenum dioxide, reaching its maximum at t = 30 min. Lastly, the further reduction of MoO_2 to metallic molybdenum proceeds until only the reflections of molybdenum are noticeable after 58 min.

The relative progression of the reduction of the molybdenum trioxide sample containing 120 µg K^+/g MoO_3 is similar. Firstly, the molybdenum trioxide is reduced to molybdenum dioxide (first reflections discernable at t = 4 min). Then, as more and more MoO_2 is developed, the first reflections stemming from Mo_4O_{11} are noticeable at t = 12 min and both phases are produced simultaneously until the starting material is exhausted (t = 30 min). Afterwards, the Mo_4O_{11} is reduced to molybdenum dioxide, reaching its maximum at t = 52 min, after which the molybdenum dioxide is further reduced to the final reduction product molybdenum. The reaction is completed after 84 min.

Calculating the relative intensity ratios according to Eq. (6), the semi-quantitative phase composition was determined for MoO_3, Mo_4O_{11}, MoO_2, and Mo. The phase composition of the data depicted in Fig. 3 is plotted in Fig. 4 (top: 34 µg K^+/g MoO_3; bottom: 120 µg K^+/g MoO_3). The same experiments were conducted for samples containing 120 µg K^+/g MoO_3 at 700 °C as well. The reduction data is shown in Fig. 5 (left) and the calculated semi-quantitative phase composition in Fig. 5 (right).

In comparison to the sample reduced at 550 °C, the reduction at 700 °C commences significantly faster. Therefore, the acquisition time was reduced to 30 s, enabling a detailed observation of the reaction process. After the initial reaction of MoO_3 to MoO_2, significantly more Mo_4O_{11} (phase content ~68% after 3 min) is developed during the reduction process. After 4 min, the reduction to molybdenum dioxide is complete (phase content ~95%) and solely the reduction to metallic molybdenum commences, which is completed after 8.5 min.

4. Discussion

During the hydrogen reduction of MoO_3, the initial phase developed is MoO_2. Depending on the exact conditions (*i.e.* temperature and potassium content) hardly any (*e.g.* 550 °C; 34 µg K^+/g MoO_3) or large amounts (*e.g.* 700 °C; 120 µg K^+/g MoO_3) of Mo_4O_{11} are developed during the reduction process. In contrast to the *in situ* powder neutron diffraction experiment conducted by Lalik et al. [14,31], no excessive Mo_4O_{11} development was observed, and the general relative phase evolution was entirely different. In case of the native sample (34 µg K^+/g MoO_3; reduced at 550 °C), the Mo_4O_{11} phase only constituted a minor part of the overall phase composition (maximum phase content ~10%), which is in considerable contrast to the findings mentioned by Lalik (~85%) but in good agreement with Ressler et al. [18] (~15%). Additionally, no steady state period of the MoO_2 content was noticed. This different behavior might be caused by the different experimental setup. The experiments described above used small sample masses and relatively high hydrogen flows, while Lalik et al. used large sample masses (10 g) paired with a slow hydrogen flow limiting the reduction of MoO_3 to MoO_2, *i.e.* the first reduction step according to Eq. (8).

Overall, the reaction proceeds through three distinct phases. At first, an incubation period occurs, during which the starting material is converted to molybdenum dioxide. Then, with an increasing fractional content of MoO_2, the formation of Mo_4O_{11} starts and both reactions increase their reaction velocities autocatalytically. Lastly, the side product Mo_4O_{11} is reduced autocatalytically to form the reaction product of this first reduction step. Starting with a MoO_3 content of $3.48 \cdot 10^{-5}$ mol (~5 mg, *i.e.* the experimental sample size), the reductions were simulated according to the mechanisms described in Table 1.

Fig. 4 and Fig. 5 (right) show both the experimentally determined data points (squares) and their respective simulated curves (fragmented lines). For all reductions the reaction constants k_x and catalytic reaction constants k_{xc} were determined. The obtained values are listed in Table 2. The sigmoidal shape of the experimental curves is well replicated by the catalytic reduction processes, which seem to be important for all

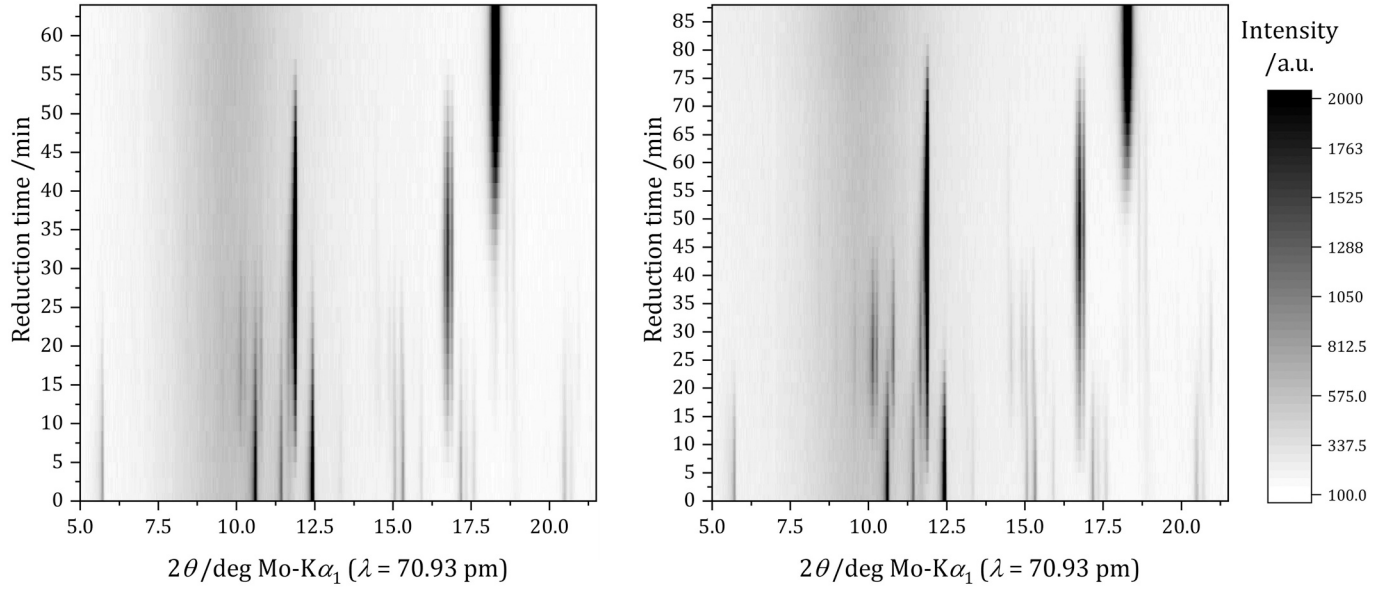

Fig. 3. Raw data heat-map of the reduction of a MoO_3 sample containing 34 (left) and 120 (right) µg K^+/g MoO_3 at T = 550 °C.

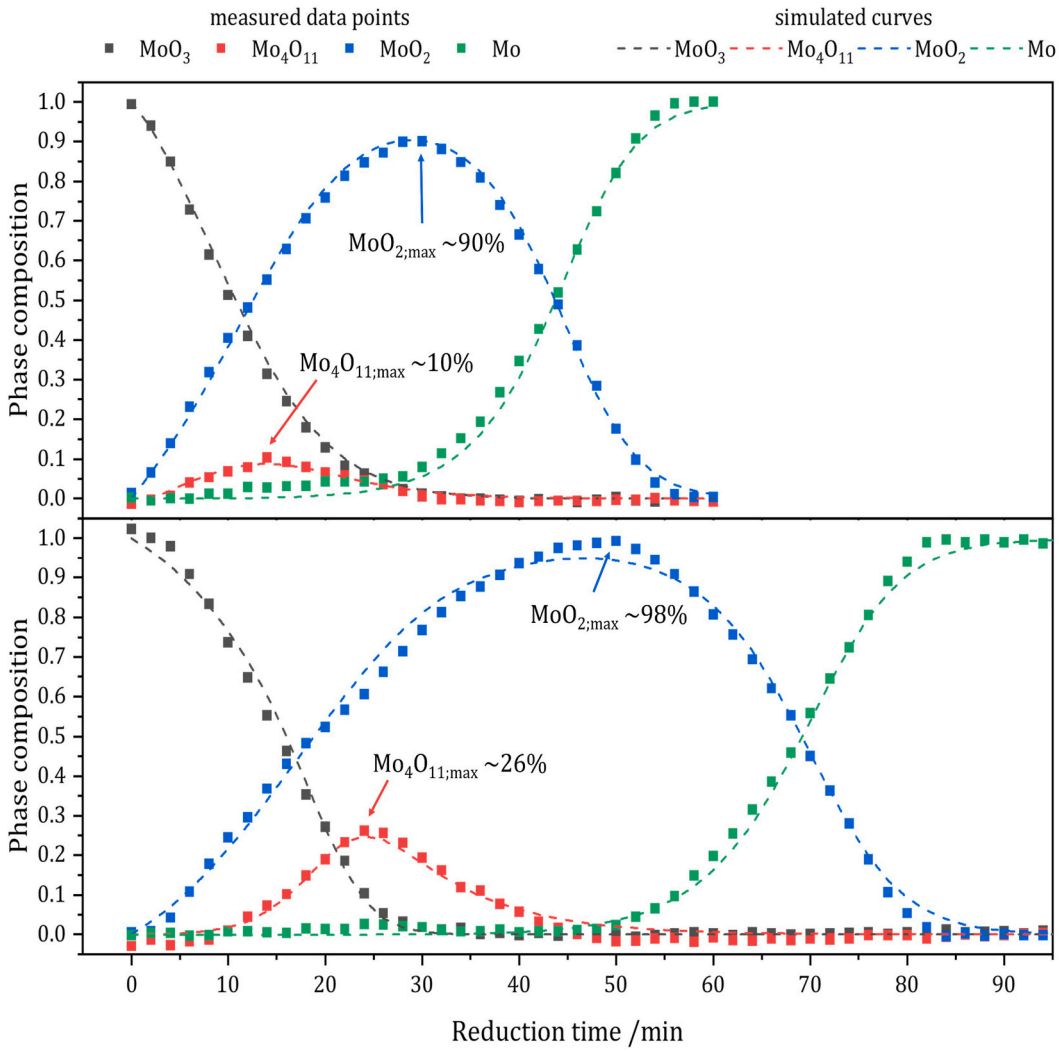

Fig. 4. Diagram of the semi-quantitative phase composition during the hydrogen reduction of a 34 µg K^+/g MoO_3 (top) and a 120 µg K^+/g MoO_3 (bottom) containing sample at 550 °C.

described reaction pathways. Reactions according to eqs. (8), (10), and (12) are catalyzed by molybdenum dioxide, while reactions (9) and (11) are catalyzed by $MoO_{2.75}$ (*i.e.* Mo_4O_{11}). Exemplary, the concentration change of MoO_3 in dependence on the concentration of $MoO_3 \equiv A$, $MoO_2 \equiv B$, $MoO_{2.75} \equiv C$ is shown in Eq. (13).

$$\frac{d[MoO_3]}{dt} = -k_1 \cdot A - k_{1c} \cdot A \cdot B - \frac{3}{4} k_2 \cdot A^{\frac{3}{4}} \cdot B^{\frac{1}{4}} - \frac{3}{4} k_{2c} \cdot A^{\frac{3}{4}} \cdot B^{\frac{1}{4}} \cdot C - k_4 \cdot A - k_{4c} \cdot A \cdot C \tag{13}$$

During the reduction of the sample containing 34 µg K^+/g MoO_3, the reduction solely follows the comproportionation reaction mechanism. The direct reduction of MoO_3 to Mo_4O_{11} had no significant impact on the reduction, which is in good agreement with the literature [18]. By increasing the potassium content to 120 µg K^+/g MoO_3, the reaction according to the comproportionation mechanism, see Eq. (9), is accelerated significantly. However, the reduction can't be solely described by this mechanism as the direct reduction of MoO_3 to Mo_4O_{11} becomes more important to fully describe the observed data. Both mechanisms now contribute to the formation of the intermediary product. However, as the further reduction of Mo_4O_{11} to MoO_2 is slowed, the overall content of Mo_4O_{11} observed in the course of the reduction is increased. Elevating the reaction temperature to 700 °C, the direct reduction of MoO_3 to MoO_2 has no further relevance to the overall reduction mechanism and the reaction progresses mostly through the direct reduction: $MoO_3 \rightarrow Mo_4O_{11}$. Additionally, Mo_4O_{11} is simultaneously produced by the comproportionation of MoO_3 and MoO_2.

After the reduction to molybdenum dioxide is concluded, the phase content of the final product, metallic molybdenum, is continuously increased. The MoO_2 is thereby directly reduced according to Eq. (12), yielding the final molybdenum product. While the derived reaction constants for reduction experiments conducted at 550 °C are similar, the reduction process becomes significantly faster with increasing temperatures, which is consistent with the literature [32].

Comparing the phase evolution diagram for the sample containing 34 and 120 µg K^+/g MoO_3, the overall reduction time is increased and most importantly, the amount of *in situ* developed Mo_4O_{11} is increased significantly (phase content at the Mo_4O_{11} maximum 10 and 26%, respectively). As we have reported in a previous publication [24], the increased potassium content results in a significant shift of the grain habitus from small to larger platelets and even cuboid like structures. Wang et al. [23] were able to maximize the *in situ* developed amount of Mo_4O_{11} by a temperature programmed low-high-low profile to increase the grain size of the resulting MoO_2 particles. In principle, the same is true for the reductions examined above. The Mo_4O_{11} turnover (= the

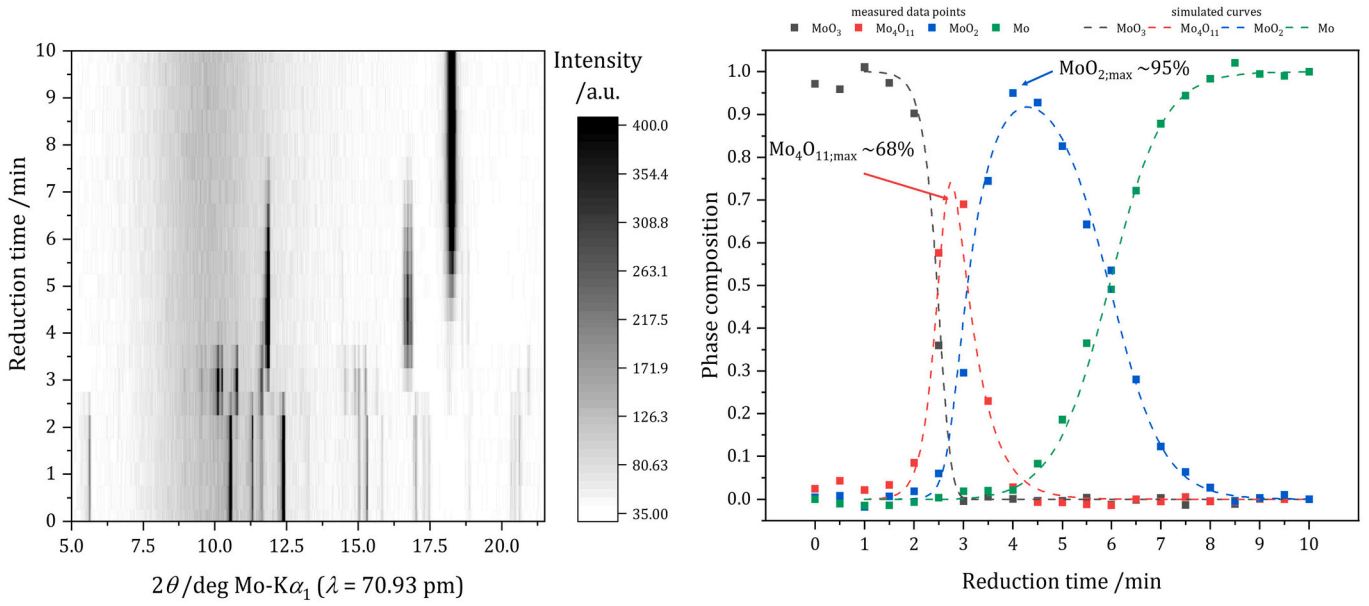

Fig. 5. Raw data heat-map of the reduction of a MoO_3 sample containing 120 µg K^+/g MoO_3 at $T = 700$ °C (left) and semi-quantitative phase composition diagram with simulated kinetic curves (right).

Table 1
Reaction equations utilized to simulate the reduction curves of the experimental data.

non-catalytic reaction	catalytic reaction	
$MoO_3 \overset{k_1}{\rightarrow} MoO_2$	$MoO_3 + MoO_2 \overset{k_{1c}}{\rightarrow} 2\,MoO_2$	(8)
$\frac{3}{4}MoO_3 + \frac{1}{4}MoO_2 \overset{k_2}{\rightarrow} MoO_{2.75}$	$\frac{3}{4}MoO_3 + \frac{1}{4}MoO_2 + MoO_{2.75} \overset{k_{2c}}{\rightarrow} 2MoO_{2.75}$	(9)
$MoO_{2.75} \overset{k_3}{\rightarrow} MoO_2$	$MoO_{2.75} + MoO_2 \overset{k_{3c}}{\rightarrow} 2\,MoO_2$	(10)
$MoO_3 \overset{k_4}{\rightarrow} MoO_{2.75}$	$MoO_3 + MoO_{2.75} \overset{k_{4c}}{\rightarrow} 2\,MoO_{2.75}$	(11)
$MoO_2 \overset{k_5}{\rightarrow} Mo$	$2\,MoO_2 \overset{k_{5c}}{\rightarrow} Mo + MoO_2$	(12)

Table 2
Reaction velocities obtained from different reduction parameters (k_x/k_{xc} in [s^{-1}] and [$mol^{-1}{\cdot}s^{-1}$]).

K^+ content of MoO_3 sample	Reduction temperature	k_1/k_{1c}	k_2/k_{2c}	k_3/k_{3c}	k_4/k_{4c}	k_5/k_{5c}
34 µg/g	550 °C	0.55/1.6	0.35/3	0/3.5		0.01/3.85
120 µg/g	550 °C	0.27/1.7	0.025/4	0/1.7	0/7	0.0045/3.2
120 µg/g	700 °C		0/90	0.35/35	0.05/90	0.25/30

sum of all Mo_4O_{11} formations during the reduction) increases with the potassium content and reduction temperature from 30% (34 µg K^+/g MoO_3; 550 °C) to 45% (120 µg K^+/g MoO_3; 550 °C) and 109% (120 µg K^+/g MoO_3; 700 °C). That is, the majority of MoO_2 produced when reducing the sample containing 34 µg K^+/g MoO_3 at 550 °C is never converted to Mo_4O_{11}, while the MoO_2 produced from the sample containing 120 µg K^+/g MoO_3 at 700 °C is converted to Mo_4O_{11} in most cases and occasionally even multiple times (compare reduction velocity constants for direct formation of Mo_4O_{11} from MoO_3 and comproportionation). In the case of the sample reduced at 700 °C, the formed MoO_2 instantaneously reacts with MoO_3 to form Mo_4O_{11}.

5. Conclusion

Utilizing the *in situ* X-ray powder diffraction setup and different sample compositions, further light was shed on the complex mechanisms of the hydrogen reduction of molybdenum trioxide to molybdenum dioxide/metallic molybdenum. The temperature dependent shift from an intermediary formation of Mo_4O_{11} solely by comproportionation at lower reduction temperatures to a mixed mechanism consisting of comproportionation and direct reduction of the starting material was observed. This shift of the reaction mechanism was also observed through the increase if the potassium content of the starting material. In comparison to earlier investigations, the content of *in situ* developed Mo_4O_{11} was confirmed as a key factor in influencing the resulting molybdenum dioxide particle morphology.

Declaration of Competing Interest

Hubert Huppertz reports financial support was provided by Plansee SE (Reutte, Austria). Hubert Huppertz reports a relationship with Plansee SE (Reutte, Austria) that includes: funding grants.

Data availability

Data will be made available on request.

Acknowledgements

The authors gratefully acknowledge the support of Plansee SE (Reutte, Austria).

References

[1] K. Nakajima, H. Ohno, Y. Kondo, K. Matsubae, O. Takeda, T. Miki, S. Nakamura, T. Nagasaka, Environ. Sci. Technol. 47 (2013) 4653–4660.
[2] J.C. Védrine, Chin. J. Catal. 40 (2019) 1627–1636.
[3] J. Haber, E. Lalik, Catal. Today 33 (1997) 119–137.
[4] J.A. Shields, P. Lipetzky, JOM 52 (2000) 37–39.
[5] A.S. Aliyev, M. Elrouby, S.F. Cafarova, Mater. Sci. Semicond. Process. 32 (2015) 31–39.

[6] I. Fedotov, A. Suchkov, A. Sliva, P. Dzhumaev, I. Kozlov, R. Svetogorov, O. Sevryukov, J. Manuf. Process. 69 (2021) 142–151.
[7] J. Bolitschek, S. Luidold, M. O'Sullivan, Int. J. Refract. Met. Hard Mater. 71 (2018) 325–329.
[8] J. Dang, G.-H. Zhang, K.-C. Chou, High Temp. Mater. Proc. 33 (2014) 305–312.
[9] W.V. Schulmeyer, H.M. Ortner, Int. J. Refract. Met. Hard Mater. 20 (2002) 261–269.
[10] J. Dang, G.-H. Zhang, L. Wang, K.-C. Chou, Int. J. Refract. Met. Hard Mater. 51 (2015) 275–281.
[11] D.T. Hawkins, W.L. Worrell, Metall. Trans. 1 (1970) 271–273.
[12] J. Słoczyński, W. Bobiński, J. Solid State Chem. 92 (1991) 436–448.
[13] P. Spevack, N. McIntyre, J. Phys. Chem. 96 (1992) 9029–9035.
[14] E. Lalik, W.I. David, P. Barnes, J.F. Turner, J. Phys. Chem. B105 (2001) 9153–9156.
[15] T. Leisegang, A. Levin, J. Walter, D. Meyer, Cryst. Res. Technol. 40 (2005) 95–105.
[16] A. Borgschulte, O. Sambalova, R. Delmelle, S. Jenatsch, R. Hany, F. Nüesch, Sci. Rep. 7 (2017) 40761.
[17] T. Ressler, R.E. Jentoft, J. Wienold, M.M. Günter, O. Timpe, J. Phys. Chem. B104 (2000) 6360–6370.
[18] T. Ressler, R.E. Jentoft, J. Wienold, O. Timpe, J. Synchrotron Rad. 8 (2001) 683–685.
[19] J. Chen, Q. Wei, Int. J. Appl. Ceram. Technol. 14 (2017) 1020–1025.
[20] J. Słoczyński, J. Solid State Chem. 118 (1995) 84–92.
[21] J. Dang, G.-H. Zhang, K.-C. Chou, R.G. Reddy, Y. He, Y. Sun, Int. J. Refract. Met. Hard Mater. 41 (2013) 216–223.
[22] L. Wang, G.-H. Zhang, K.-C. Chou, Int. J. Refract. Met. Hard Mater. 54 (2016) 342–350.
[23] X. Wang, J. Liu, F. Zhuang, H. Zhao, L. Jing, Metall. Mater. Trans. B41 (2010) 1067–1073.
[24] M. Zoller, M. O'Sullivan, H. Huppertz, Chem. Eur. J. 27 (2021) 18141–18149.
[25] L. Kihlborg, Ark. Kemi 21 (1963) 357.
[26] S. Åsbrink, L. Kihlborg, Acta Chem. Scand. 18 (1964) 1571–1573.
[27] E.R. Jette, F. Foote, J. Chem. Phys. 3 (1935) 605–616.
[28] H. Negishi, S. Negishi, Y. Kuroiwa, N. Sato, S. Aoyagi, Phys. Rev. B 69 (2004), 064111.
[29] R. Roy, D.K. Agrawal, H.A. McKinstry, Annu. Rev. Mater. Sci. 19 (1989) 59–81.
[30] K. Inzani, M. Nematollahi, S.M. Selbach, T. Grande, F. Vullum-Bruer, Thin Solid Films 626 (2017) 94–103.
[31] E. Lalik, Catal. Today 169 (2011) 85–92.
[32] B.-S. Kim, E.-Y. Kim, H.-S. Jeon, H.-I. Lee, J.-C. Lee, Mater. Trans. 49 (2008) 2147–2152.